A Topological Study of the Decomposition of 6,7,8-Trioxabicyclo[3.2.2]nonane Induced by Fe(II): Modeling the Artemisinin Reaction with Heme

Pamela Moles,[†] Mónica Oliva,[†] Ángel Sánchez-González,[‡] and Vicent S. Safont*,[†]

Departament de Química Física i Analítica, Universitat Jaume I, Avda. Sos Baynat s/n, 12071 Castelló, Spain, and Departamento de Química Orgánica, Grupo de Modelización y Diseño Molecular, Facultad de Ciencias, Universidad de Granada, E-18071, Granada, Spain

Received: October 26, 2009; Revised Manuscript Received: December 1, 2009

We report a theoretical study on the electronic and topological aspects of the reaction of dihydrated $Fe(OH)_2$ with 6,7,8-trioxabicyclo[3.2.2]nonane, as a model for the reaction of heme with artemisinin. A comparison is made with the reaction of dihydrated ferrous hydroxide with O_2, as a model for the heme interaction with oxygen. We found that dihydrated $Fe(OH)_2$ reacts more efficiently with the artemisinin model than with O_2. This result suggests that artemisinin instead of molecular oxygen would interact with heme, disrupting its detoxification process by avoiding the initial heme to hemin oxidation, and killing in this way the malaria parasite. The ELF and AIM theories provide support for such a conclusion, which further clarifies our understanding on how artemisinin acts as an antimalarial agent.

Introduction

Malaria is nowadays the most lethal parasitic disease, causing more than one million deaths yearly,[1−4] most of them children under age 5, in more than 100 nations.[5,6] It is caused by the members of the genus *Plasmodium* that infect humans through the bite of the female Anopheles mosquito. The *Plasmodium* sporozoites invade hepatocytes and develop to release merozoites, which in turn invade erythrocytes, where they grow to mature trophozoites, then to schizonts, and finally to release more merozoites that invade more erythrocytes closing the cycle.[7] To sustain its rapid development, the malaria parasite must synthesize its own proteins, and digestion of host hemoglobin within the red blood cells serves as the major amino acids source. It is known that *Plasmodium falciparum* digests between 60% and 80% of the hemoglobin present in the infected erythrocytes.[8,9] This process gives globin fragments that are further hydrolyzed into amino acids, and takes place in an acidic (pH 5.0−5.4) organelle within the parasite, called the food vacuole, that contains proteolytic enzymes.[10]

Digestion of hemoglobin within the food vacuole also releases free heme (Fe(II) protoporphyrin-IX, Scheme 1), which is toxic for the parasite due to its ability to destabilize and lyse membranes and to inhibit the activity of several enzymes.[11] Thus, a concomitant detoxification process of heme is necessary for the parasite to uninterruptedly grow and proliferate. It has recently been shown that at least 95% of the released free heme is detoxified by its conversion into hemozoin, the malarial pigment, which is an insoluble crystalline material.[8,12] The hemozoin formation involves the heme oxidation to hemin (Fe(III) protoporphyrin-IX) by a mechanism that is not yet fully explored but that is presumed to involve molecular oxygen as the oxidant agent, followed by the formation of hemin dimers (β-hematin) which finally assemble to form the hemozoin crystal.[8]

SCHEME 1

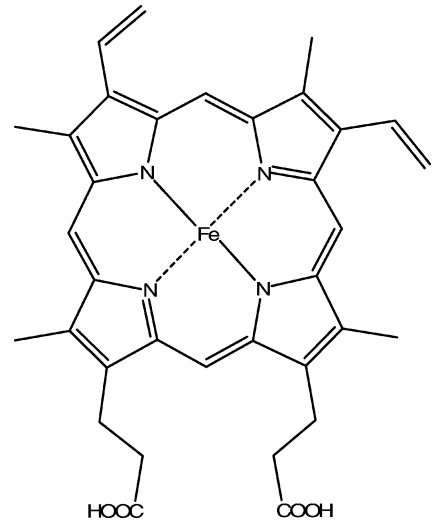

Disruption of the hemozoin formation is the strategy most widely used for treating malaria.[13] Quinoline-based antimalarials act by forming adducts with free heme resulting in the prevention of heme polymerization to nontoxic hemozoin.[14−17]

While the malaria parasites are becoming resistant to quinoline-based antimalarial agents, such as chloroquine, and even to quinine and mefloquine,[18,19] artemisinin (Scheme 2) remains the most potent and rapidly acting antimalarial drug against resistant strains of *Plasmodium falciparum* at hand nowadays.[20] Combinations of artemisinin with other antimalarial drugs are now recommended treatments for severe malaria in the most endemic areas,[21] because such combinations might be useful in delaying the emergence of artemisinin resistance.[22]

Artemisinin is a sesquiterpene lactone with an endoperoxide group, and its 1,2,4-trioxane ring system has been proven to be critical for the antimalarial activity.[4,23] It has been suggested that interaction with heme produces carbon-centered radical intermediates, which can cause the parasite death.[3,4,7,14,15,24−29] Definitive evidence for the generation of carbon radical inter-

* To whom correspondence should be addressed. E-mail: safont@qfa.uji.es. Tel: 34964728085. Fax: 34964728066.
[†] Universitat Jaume I.
[‡] Universidad de Granada.

10.1021/jp910207z
Published on Web 12/22/2009

SCHEME 2

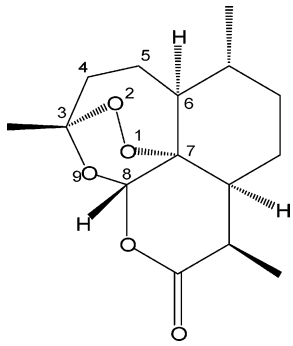

mediates during ferrous-mediated endoperoxide degradation of artemisinin and its derivatives was provided by EPR spin-trapping techniques.[30−32] Such carbon radicals have been reported as heme alkylating agents in vivo in infected mice,[24,25] disrupting in this way the heme detoxifying process and leading to the parasite death by a mechanism similar to that proposed for the quinoline-based antimalarials.[14−17] Although some studies suggested that the activity of artemisinins does not require heme,[33−36] it has been pointed out that these studies used iron chelators capable of chelating heme iron as well and that the claims about artemisinin's effect not requiring heme can be considered as premature.[11]

Apart from heme, other molecular targets have been proposed for the reactive intermediates generated from artemisinin and its derivatives.[33,37−42] Overall, the weight of evidence and the fact that resistance to the artemisinins has not yet developed suggest that the drugs do not exert their antimalarial effects by hitting a single biological target, but rather by simultaneously hitting several targets with very high precision and efficiency.[2,34]

The decomposition mechanism of artemisinin and other trioxanes induced by Fe(II)-containing species has been the subject of several studies during the past decade. With slight modifications, the unified mechanism proposed by Cumming[43] and Wu[32] has been generally accepted as reference framework, and a series of theoretical investigations related with the antimalarial mode of action of artemisinin have been reported.[1,6,7,18,23,44−62]

Recently, it has been established that heme reacts with artemisinin more efficiently than hemin, inorganic iron, or hemoglobin,[63] although previous studies suggested that ferrous (but not ferric) hemoglobin reacts with artemisinin much faster than free heme.[11] In any case, these studies revealed that hemin reacts very slowly with artemisinin, and hence it can be hypothesized that once heme is oxidized to hemin, the detoxification process to hemozoin would take place even in the presence of artemisinin. Thus, the disruption of the hemozoin formation process by artemisinin must take place before the Fe(II) to Fe(III) oxidation. The possibility of artemisinin competing with molecular oxygen in the very first step of hemozoin formation has not been fully explored to date.

To gain a deeper insight into the reaction between artemisinin and heme, it is very convenient to envisage a sound analysis at the electronic level. To this end, the electron localization function (ELF), defined by Becke and Edgecombe,[64,65] is the basis of the electron-density-based topological analysis and provides useful information on the bond structure. On the other hand, the atoms in molecules (AIM) theory explores the topology of the electron density and describes accurately the chemical concepts of atom, bond and structure.[66,67] In the framework of this approach, bond critical points (BCP) of each compound are located, and the electron density at these points offers quantitatively valid information on the strength and the character of the linkage.

In this paper, we report a study on electronic and topological aspects of the reaction of heme with artemisinin by using very simple molecular models. A comparison is made with the reaction of heme with molecular oxygen with the aim of testing the competitive hypothesis and to shed additional light to our current understanding of the antimalarial mode of action of artemisinin and its derivatives.

Computational Methods and Models

The aim of the present work is to focus on the interaction of Fe(II) with the endoperoxide bridge of artemisinin, and also with molecular oxygen. To this end, we have selected very simple models that allow us to reveal the electronic details of such interactions and to maintain the computational times in a reasonable range. Therefore, artemisinin has been modeled with 6,7,8-trioxabicyclo[3.2.2]nonane (**1f**), while heme (Fe(II) protoporphyrin-IX) has been modeled by dihydrated $Fe(OH)_2$ (**2f**) (Scheme 3).

The interaction between heme and artemisinin can give rise to two oxygen-centered radicals that further evolve to carbon-centered radical species. These species have been reported as mediators for the disruption of the heme detoxifying process and the subsequent parasite death, as stated above. Hence, the study herein reported mainly deals with the electronic and topological aspects of the steps leading from the model reactants, **1f** plus **2f**, to the model carbon-centered radicals **5f** and **6f** (see Scheme 3). On the other hand, the interaction between heme and molecular oxygen has been modeled with **2f** and O_2.

The calculations have been done at the B3LYP theoretical level with the 6-311+G(d,p) basis set, using the Gaussian03 program.[68] This method includes Becke's three-parameter nonlocal hybrid exchange potential[69] and the nonlocal correlation functional of Lee, Yang, and Parr.[70] All stationary points shown in Scheme 3 have been fully optimized and characterized as minima or transition structures (TS) by means of a vibrational analysis. For the minima, all the wavenumbers are positive, while for the TS there is only one imaginary wavenumber. This imaginary frequency is associated to the transition vector (TV)[71] and describes the atomic motions at TS. It can be used to trace the intrinsic reaction coordinate (IRC)[72] pathway from each TS to its associated minima, i.e., to the *reactant* and *product* of each individual step.

Most of the species appearing along the studied steps have unpaired electrons. In these cases the unrestricted (UB3LYP) formalism has been used. We have calculated the energy of the stationary points (except **1f** and O_2) as a function of its electronic state, and we have found that the quintuplet state is the most stable electronic state in all cases except the interaction complex between **2f** and oxygen (**C3***)*, which is a septuplet.

The topological analysis of the gradient vector field of ELF function is a powerful tool: the exploration of its mathematical properties enables molecular space partition into core and valence basins defined by attractors in which the ELF function shows a high value. The valence basins are characterized by their synaptic order, i.e., by the number of core basins that show frontier with the valence basin. ELF ($\eta(r)$) is interpreted as a measure of the electron localization in atomic and molecular systems, as the probability of finding two paired electrons. Values above 0.5 indicate a localized character, while values below 0.5 correspond to delocalized electron density. From a

SCHEME 3

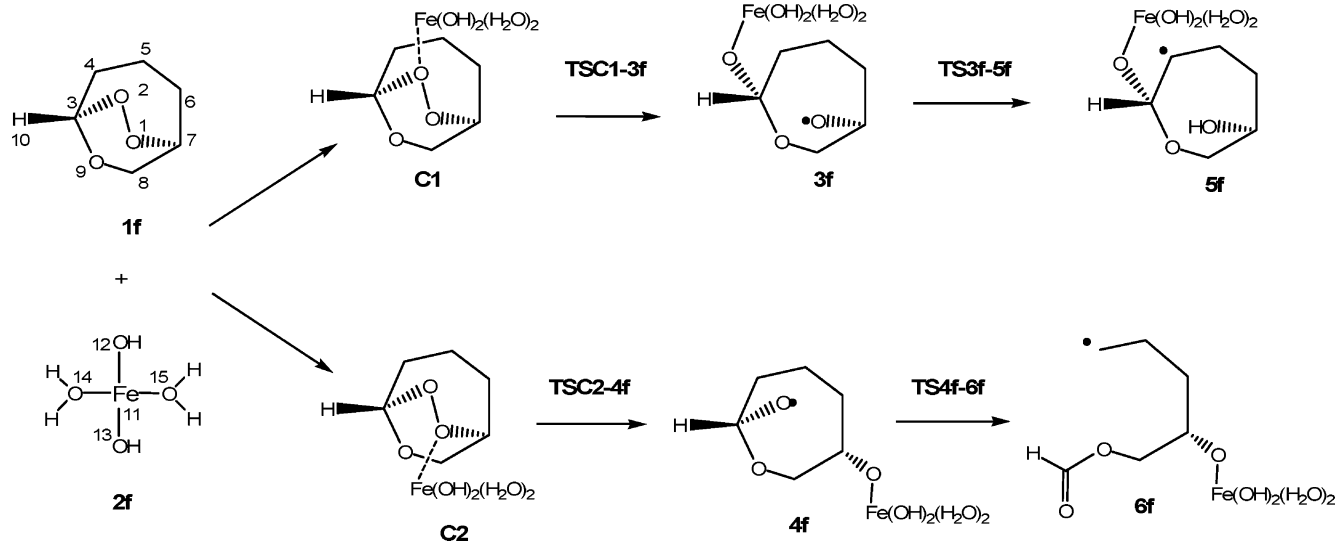

quantitative point of view, the method integrates the electron density over the basins to have the basin populations.

On the other hand, the AIM theory can be used to analyze the main characteristics of the bonds that participate in a chemical reaction, through evaluation of the properties of the corresponding BCP. The electron density ($\rho(r)$) of a BCP is related to the bond strength. To some extent, it also measures the bond multiplicity, although this analysis must be performed with care, because the density may be influenced by other phenomena. The electronic energy density ($E_d(r)$) provides information about bond stability: highly negative values involve stable bonds. The values of the Laplacian of the electron density ($\nabla^2\rho(r)$) indicate concavity or convexity depending on its negative or positive sign, respectively. Negative values of $\nabla^2\rho(r)$ indicate valence shell charge concentration regions, while positive values are found in valence shell charge depletion zones. Thus, an unshared-electron (or electrostatic) interaction is characterized by low values of $\rho(r)$ and positive values of $\nabla^2\rho(r)$ at the BCP, whereas high values of $\rho(r)$ and negative values of $\nabla^2\rho(r)$ correspond to a shared-electron (or covalent) interaction.

The AIM and ELF analyses have been carried out from the computed B3LYP/6-311+G(d,p) electron density, with the AIM2000[73] and TopMoD[74] software packages, respectively, and the ELF isosurfaces have been visualized with the AMIRA 4.1 program.[75] The ELF isosurfaces are plotted at a value of 0.815 for **1f**, **TSC1-3f**, and **TSC2-4f** structures, and at a value of 0.784 for the other species, as they are the optimal values to properly depict the basins. To visualize the small basin between the peroxide oxygens in **1f**, **C1**, and **C2**, a value of 0.665 for the isosurface has been required. The same value has been used for the monosynaptic basin at C4 in **6f**. The color convention represents core basins in magenta, and the remaining valence basins are classified depending on their synaptic order: red for monosynaptic, green for disynaptic and gray for hydrogenated basins.

Results and Discussion

We have studied the steps involved in the C-radical formation, shown in Scheme 3, using **1f** as artemisinin model and **2f** as heme model, as stated above.

By approaching **2f** to the O2 atom of **1f**, an interaction complex, **C1**, can be found. Such species is calculated to be 13.03 kcal/mol more stable than the starting separated reactants, showing the affinity between Fe(II) and the peroxidic oxygen atoms (see Figure 1, where the structures are depicted, and Figure 2, where the energetic profile is sketched). From this point, a transition structure can be found (**TSC1-3f**), lying 2.78 kcal/mol above the aforementioned complex. Following the IRC pathway from **TSC1-3f**, the O1-centered radical **3f** is found 39.62 kcal/mol below the reactants. As can be seen in Figure 1, the O1−O2 distance increases as the Fe atom approaches O2, evolving from 1.48 Å at **1f** to 3.57 Å at **3f**, while the Fe−O1 distance shortens to 1.83 Å at **3f**. At the interaction complex, these distances are 1.49 and 2.23 Å, respectively, while at the TS the corresponding values are 1.66 and 2.00 Å.

On the other hand, if **2f** approaches the O1 atom of **1f**, the complex **C2** is found 9.64 kcal/mol below the starting reactants. The **TSC2-4f** lies 1.77 kcal/mol above the complex, and the O2 centered radical **4f** is found 42.51 kcal/mol below the reactants (see Figure 2). In this case the O1−O2 distance is 1.49 Å at the interaction complex, 1.63 Å at the corresponding TS, and 3.27 Å at **4f**, while the Fe−O2 distance is 2.21 Å at the complex, 2.03 Å at the TS, and 1.82 Å at **4f** (see Figure 1).

From **3f**, a moderate activation barrier of 12.81 kcal/mol has to be surmounted for reaching the secondary C4 radical **5f**, which is slightly more stable than **3f**. The **TS3f-5f** is associated to the H migration from C4 to O1. It can be sensed in Figure 1 the motion of the H atom from C4 to O1 on going from **3f** to **5f**: the H−C4 distance is 1.10, 1.26, and 2.58 Å at **3f**, **TS3f-5f**, and **5f**, respectively, while the H−O1 distance shortens from 2.21 Å at **3f** to 1.29 Å at **TS3f-5f** and finally to 0.97 Å at **5f**.

From **4f** a very small activation barrier of 2.08 kcal/mol is found in the way to the C4 primary radical **6f**, which is the most stable species found in this work. The **TS4f-6f** is associated to the breaking of the C3−C4 bond, as can be seen in Figure 1, where the C3−C4 distances are reported at **4f** (1.63 Å), then at **TS4f-6f** (1.95 Å) and at **6f** (4.25 Å), with this bond completely broken. The energetic values obtained support the O2 radical route to be preferred from both a thermodynamic and a kinetic point of view. Hence the O2 radical route will prevail, which is in agreement with the in vivo experiments since the only fully characterized alkylation reaction reported to date in infected mice is the heme alkylation by means of the C4 primary radical.[24,76]

On the other hand, when **2f** approaches molecular oxygen, an interaction complex (**C3**, see Figure 3) is formed with no

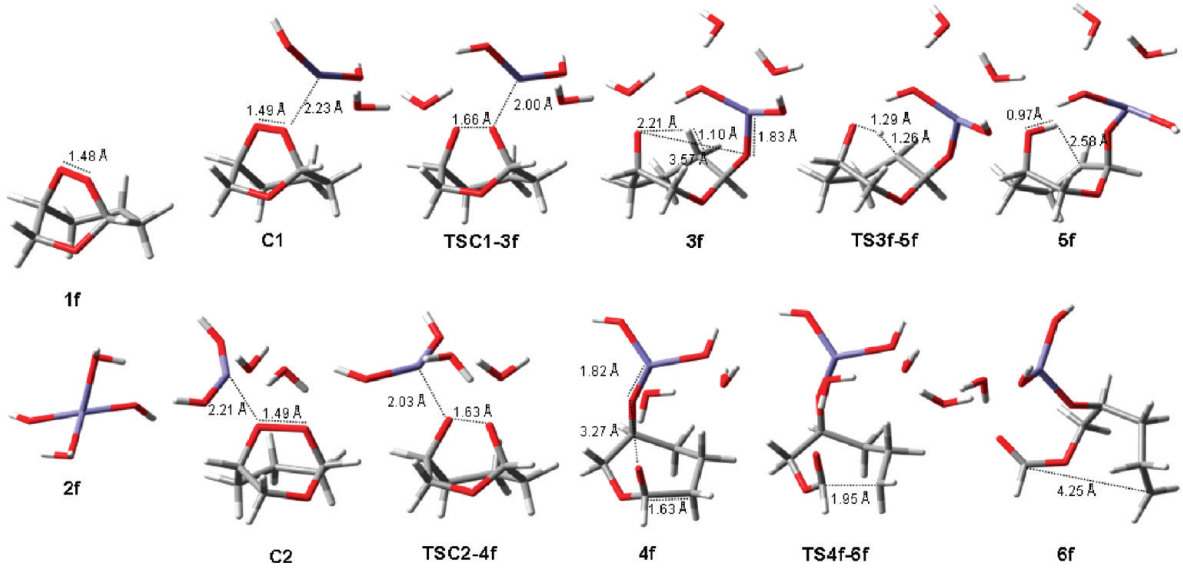

Figure 1. Structures of the indicated stationary points. Selected distances (Å) are included.

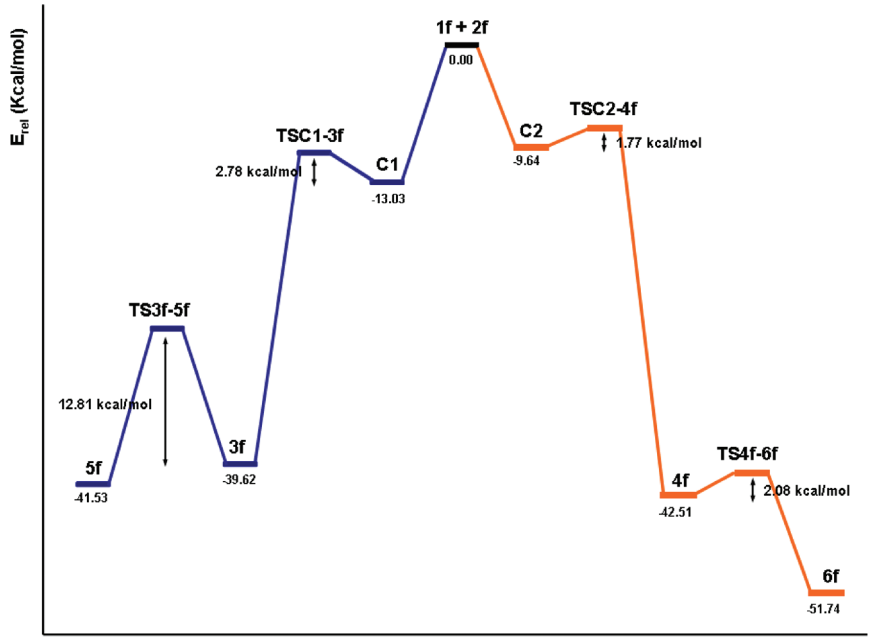

Figure 2. Relative energy (kcal/mol) profiles. Total energy of the reference point (**1f** plus **2f**): −2028.772 368 hartree.

noticeable activation barrier. However, the stabilization achieved is much lesser than the one obtained with the formation of **C1** or **C2**: the most stable complex has septuplet electronic state and lies only 2.42 kcal/mol below the separated reactants, i.e., below **2f** in its quintuplet state and O_2 in its fundamental triplet electronic state. Therefore, the ferrous model reacts preferably with the endoperoxide-containing species than with molecular oxygen. If this finding could be extrapolated to the actual system, artemisinin instead of molecular oxygen would interact with heme. Hence the initial heme to hemin oxidation would be avoided, disrupting in this way the heme detoxification process.

Topological Description of 1f and 2f. The ELF analysis of **1f** indicates that the O1−O2 peroxide bond is electron deficient: two monosynaptic basins with low populations of 0.26 and 0.28 electrons are found between O1 and O2. On the contrary, the basins corresponding to the unshared pairs of these oxygen atoms present high populations, more than 2.5 electrons for each

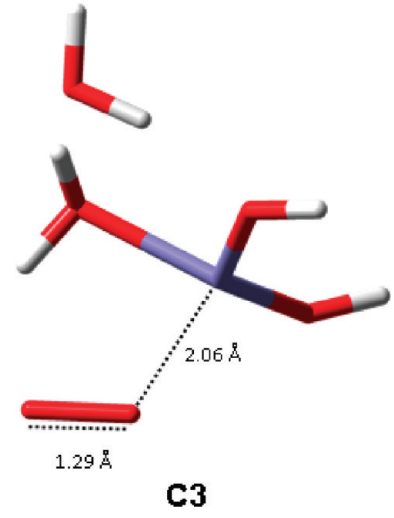

Figure 3. Structure of **C3**.

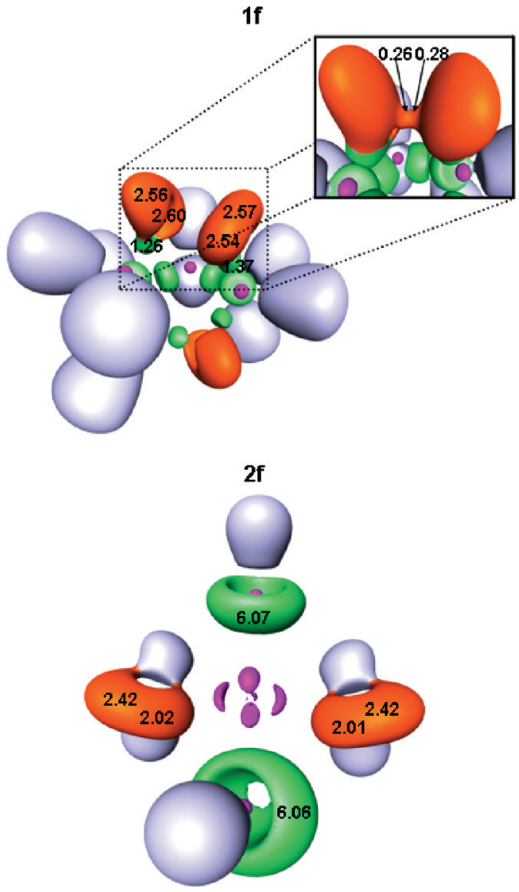

Figure 4. ELF isosurfaces of **1f** and **2f**.

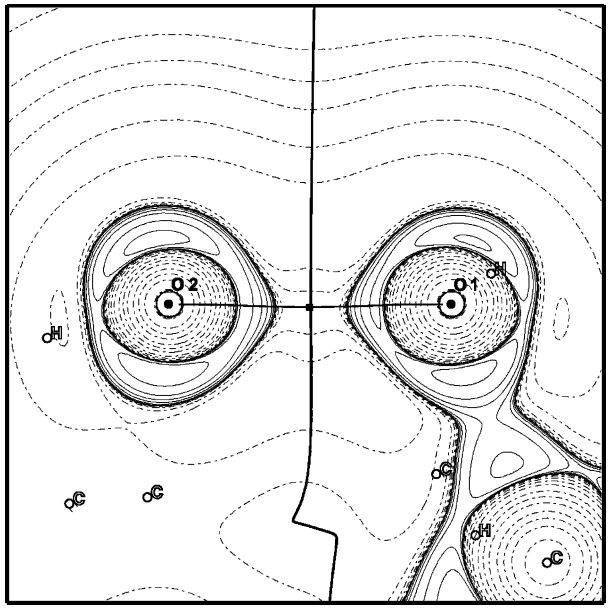

Figure 5. Contour map of the Laplacian of the electron density for **1f**.

basin. These results show that the low population of the peroxide basins causes the increase of charge on lone pairs; see Figure 4.

The **1f** Laplacian map of electron density (Figure 5) reveals that the BCP of the peroxide bond is located in a wide region of charge depletion. It is shown as well by the Laplacian ($\nabla^2\rho(r)$) positive value of 0.121 au in this critical point (Table 1). The positive value of $\nabla^2\rho(r)$ and the value of −0.152 au for the

TABLE 1: Electronic Properties of Selected Bond Critical Points (BCP) for the Indicated Species

	bond	$\rho(r)$ (au)	$\nabla^2\rho(r)$ (au)	$E_d(r)$ (au)
1f	O1−O2	0.255	0.121	−0.152
2f	Fe−O12	0.111	0.615	−0.020
	Fe−O13	0.111	0.622	−0.020
	Fe−O14	0.038	0.179	0.000
	Fe−O15	0.038	0.179	0.000
C1	O1−O2	0.250	0.140	−0.145
	O2−Fe	0.043	0.239	0.002
TSC1-3f	O1−O2	0.156	0.343	−0.045
	O2−Fe	0.075	0.456	−0.001
3f	O1−O2	–	–	–
	O2−Fe	0.118	0.687	−0.023
	C4−H	0.274	−0.905	−0.270
	O1−H	0.016	0.062	0.003
TS3f-5f	C4−H	0.176	−0.352	−0.130
	O1−H	0.145	0.030	−0.081
5f	C4−H	–	–	–
	O1−H	0.353	−0.240	−0.682
C2	O1−O2	0.248	0.145	−0.143
	O1−Fe	0.045	0.253	0.002
TSC2-4f	O1−O2	0.168	0.328	−0.056
	O1−Fe	0.071	0.421	−0.001
4f	O1−O2	–	–	–
	O1−Fe	0.125	0.706	−0.029
	O2−C3	0.337	−0.395	−0.521
	C3−C4	0.188	−0.309	−0.126
TS4f-6f	O2−C3	0.378	−0.329	−0.616
	C3−C4	0.090	−0.006	−0.034
6f	O2−C3	0.410	−0.171	−0.690
	C3−C4	–	–	–
O_2	O−O	0.539	−0.765	−0.659
C3	O−O	0.424	−0.317	−0.419
	Fe−O	0.080	0.314	−0.006

electronic energy density ($E_d(r)$) indicate that the bond stability is relatively low. On the other hand, the electron density ($\rho(r)$) in this BCP is 0.255 au, pointing out that even with a small value for $E_d(r)$ and being in a charge depletion zone, this bond can be described as a shared-electron interaction, as the ELF isovalue picture reflects. Hence, the O1−O2 peroxide bond can be described by the valence domains (the unshared basins of each oxygen), and by a small domain that is separated into two monosynaptic basins at an ELF value of ca. 0.74. This is in agreement with the work by Sambrano et al.,[77] who analyzed a different system containing a peroxide bond and the prototype peroxide-containing molecule, O_2^{2-}. They also found two monosynaptic basins placed between the oxygen core basins at a value of 0.74 for the ELF function. From the point of view of the catastrophe theory, such topology of ELF, early observed in studies of the F_2 molecule by Llusar et al.,[78] corresponds to a forming/breaking of the bond via the cusp catastrophe; therefore, the name "protocovalent bond" has been proposed. This kind of bond has been identified in other systems containing a peroxide bond.[79]

In **2f** a disynaptic basin of about six electrons can be found between each hydroxyl oxygen atom and the Fe atom (see Figure 4). The oxygen atoms of the water molecules present two monosynaptic basins with about two electrons, corresponding to the lone pairs. The bonds between the hydroxyl oxygens and Fe present a positive value of $\nabla^2\rho(r)$, meaning that the BCP are located in a charge depletion region, even though the value of 0.111 au for $\rho(r)$ and the small but negative value of $E_d(r)$ demonstrate the bond formation. With regard to the water oxygens and their interactions with Fe, the BCP are also located in a charge depletion zone, but $\rho(r)$ presents smaller values and

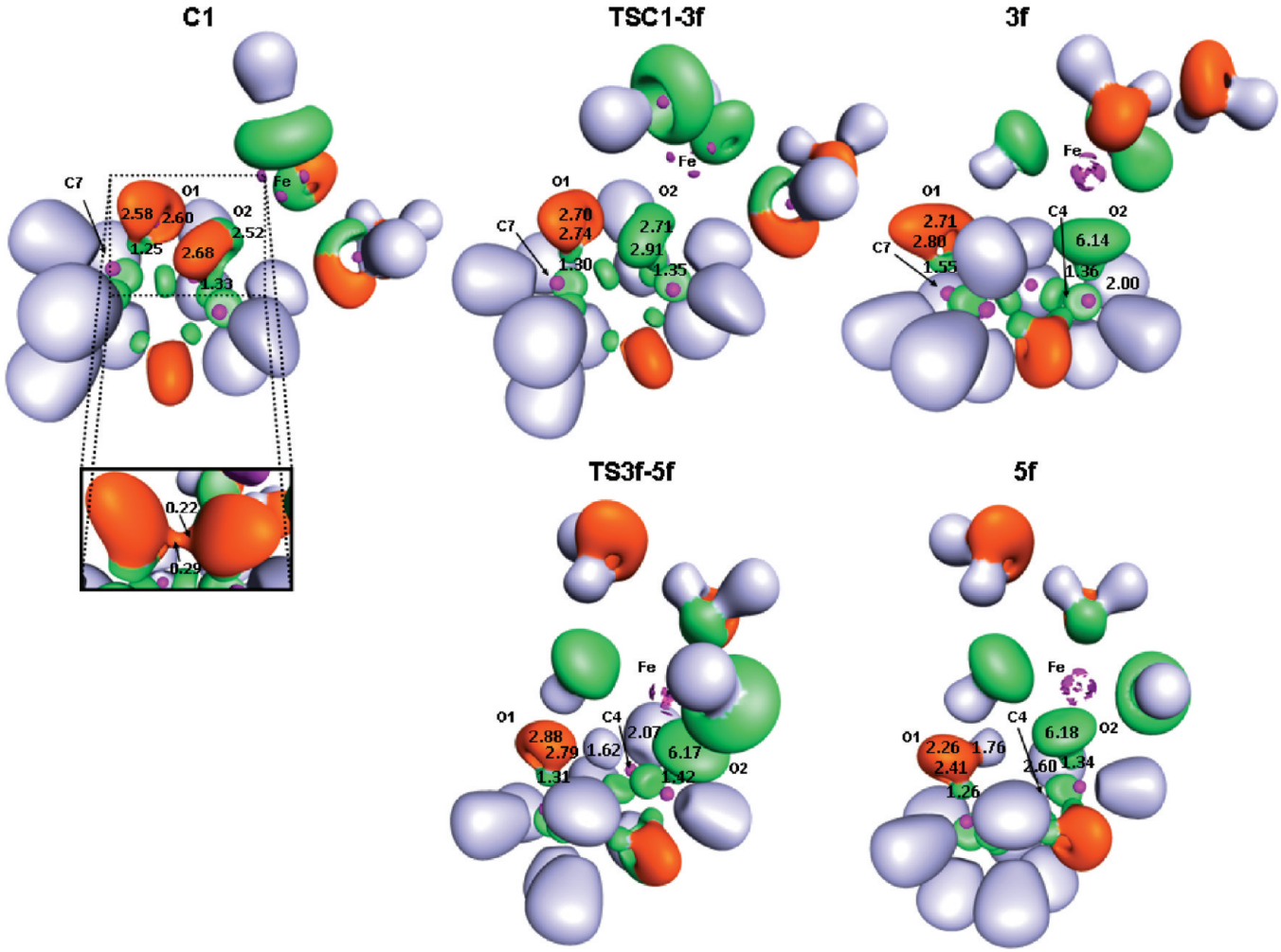

Figure 6. ELF isosurfaces of **C1**, **TSC1-3f**, **3f**, **TS3f-5f**, and **5f**.

$E_d(r)$ is zero, showing that these interactions are weaker than the bonds between the hydroxyl oxygens and Fe.

Topological Description of C1, TSC1-3f, and 3f. The monosynaptic basins corresponding to the peroxide bond can still be found at **C1**, and they disappear at **TSC1-3f** (Figure 6), showing the peroxide bond cleavage. The shape of the basins for both oxygens is the same in **C1** and **TSC1-3f** as in **1f**, and hence the proximity of the Fe atom to O2 does not significantly change the structure of the oxygen unshared basins. One of the O2 unshared basins presents monosynaptic order at **C1**, while both basins are disynaptic at the TS: this is shown by the color change from red to green in Figure 6. At **3f**, with the Fe atom linked to O2, there is only one disynaptic basin between Fe and O2, with a different shape. Hence, with regard to the Fe−O2 bond, the **TSC1-3f** has reactant-like character.

On the other hand, the increase of the population of the unshared basin in O1 at **TSC1-3f** with respect to **C1**, as well as the disappearance of the basins between the oxygen atoms, indicates that **TSC1-3f** is productlike regarding the O1−O2 bond. It is shown in this way that the cleavage of the peroxide bond initiates the electronic reorganization leading from the reactants to the O-centered radical **3f**.

The ELF study of **3f** (Figure 6) shows a different topology for the oxygens O1 and O2, compared with **1f**, **C1**, and **TSC1-3f**, since O2 is bound to Fe. The peroxide bond has been broken and O1 shows overpopulated unshared basins with 2.80 and 2.71 electrons. These populations, far larger than two electrons each, indicate that O1 takes electrons coming from the peroxide bond breaking. In addition, it can be seen that the population of the disynaptic basin between O1 and C7 increases from 1.25 at **C1** to 1.55 at **3f**, thus giving theoretical grounds to the radical character of O1.

The AIM analysis (Figure 7 and Table 1) describes the O2−Fe bond formation and the peroxide bond cleavage in the reaction path connecting **C1** and **3f**. The BCP between O2 and Fe presents a low value of $\rho(r)$ at **C1**. This value increases at **TSC1-3f**, and further increases at **3f**, showing the O2−Fe bond formation. The $E_d(r)$ for this BCP has a positive value of 0.002 au in **C1**, and it goes to a negative value (−0.001 au) at the transition state and −0.023 au at **3f**, also indicating a strengthening of the Fe−O2 bond. On the other hand, the cleavage of the peroxide bond is described by the drop in $\rho(r)$ values, which go from 0.250 au in **C1** to 0.156 au in the transition state, while in **3f** no BCP has been found between the two oxygen atoms. Furthermore, the $E_d(r)$ reveals the loss of stability of this peroxide bond, going from −0.145 au in **C1** to −0.045 au in the transition state.

Topological Description of TS3f-5f and 5f. The ELF analysis of **TS3f-5f** shows that the O2 atom remains bound to Fe with the valence shell of the oxygen completely in contact with the core basins of Fe atom, as can be deduced from the disynaptic basin between O2 and Fe, with a population of 6.17 electrons (Figure 6). Furthermore, there is a hydrogenated basin between O1 and C4 with a population of 1.62 electrons. This basin accounts for the H transfer from C4 to O1 in this step. The unshared basins of the O1 oxygen present high populations

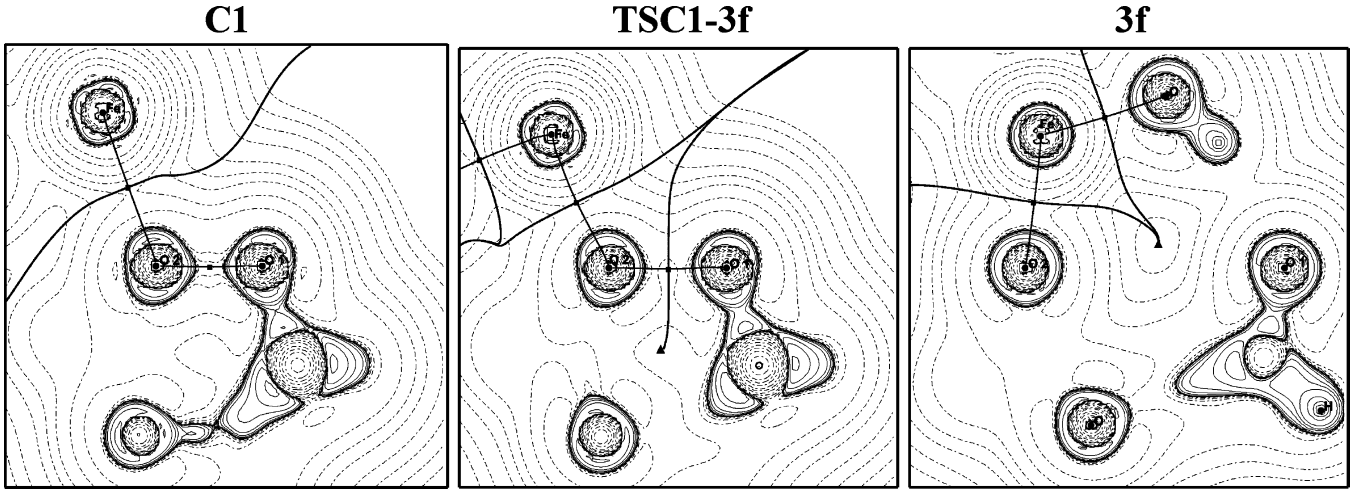

Figure 7. Contour maps of the Laplacian of the electron density for the indicated stationary points.

of 2.88 and 2.79 electrons, indicating that the O1 atom carries the electronic excess.

On the other hand, at **5f** the unshared basins of O1 present a population lower than at **TS3f-5f**. The difference between these populations is exactly one electron. This fact reveals that **TS3f-5f** can still be described as a radical centered in O1, while in **5f** the O1 has formed a OH group and the unpaired electron is centered in C4, as is shown by the population excess of 0.60 electrons of the only hydrogenated basin of C4 and the excess of 0.25 electrons of the disynaptic basin between C4 and C5, not shown in Figure 6. Hence, the ELF analysis nicely describes the electron flows leading from the O1-centered radical **3f** to the C4-centered radical **5f**.

The AIM study of the reaction yielding **5f** accounts for the H transfer from C4 to O1, i.e., the C4−H bond cleavage and the O1−H bond formation (see Table 1). The BCP found for the C4−H distance at **3f** has a $\rho(r)$ value of 0.274 au, while at **TS3f-5f** this value is 0.176 au. At **5f** no BCP has been found between C4 and H. The $E_d(r)$ for this BCP in **3f** is −0.270 au and increases to −0.130 au for **TS3f-5f**. Furthermore, the $\nabla^2\rho(r)$ has a less negative value of −0.352 au in **TS3f-5f**, being −0.905 au in **3f**. The increase of $\nabla^2\rho(r)$, the decrease of $\rho(r)$, and the increase of $E_d(r)$ on going from **3f** to the transition state point out the progressive C4−H bond cleavage. A BCP has been found between the atoms O1 and H for the three species (**3f**, **TS3f-5f**, and **5f**). The $\rho(r)$ in this BCP for **3f** is very small, as expected because there is no bond between these atoms. At **TS3f-5f** and **5f** this value is larger: 0.145 and 0.353 au, respectively. The $E_d(r)$ goes from 0.003 au in **3f** to a more stable value of −0.081 au in **TS3f-5f** and a much more stable value of −0.682 au in **5f**. The $\nabla^2\rho(r)$ has positive values for **3f** and **TS3f-5f**, 0.062 and 0.030 au, respectively, and a negative value for **5f**, −0.240 au. This means that at **5f** the BCP O1−H is in a charge accumulation region. All these values account for the O1−H bond formation when the reaction gives **5f** from **3f**.

Topological Description of C2, TSC2-4f, and 4f. As can be calculated from the data shown in Figure 8, on going from **C2** to **TSC2-4f** the O unshared basins increase its population in 0.34 electrons for O1 and in 0.28 for O2. The basins show the same shape for the two structures, and hence the O1−Fe interaction does not result in a change of the oxygen basins shape. At **4f**, with the Fe atom linked to O1, there is only one disynaptic basin between these two atoms, with a different shape. Therefore, with regard to the Fe−O1 bond, the **TSC2-4f** has reactant-like character.

On the other hand, at the transition state there are no basins between O1 and O2, meaning that the peroxide bond has been broken. This fact and the high population of the unshared basins of O2 indicate that the transition state resembles the product **4f** with respect to the O1−O2 bond. Hence, we find again that the cleavage of the peroxide bond initiates the electronic reorganization, leading in this case to the **4f** O-centered radical.

The ELF analysis of **4f** indicates that Fe is completely linked to O1, as the shape of the disynaptic basin between O1 and Fe shows, presenting frontier with Fe and having a population of 6.19. In addition, the two basins corresponding to the lone pairs of O2 have a population excess of 1.53 electrons, because the unshared electron is located on this oxygen. Moreover, it can be seen that the population of the disynaptic basin between O2 and C3 increases from 1.34 at **C2** to 1.65 at **4f**, in agreement with the radical character of O2 at **4f**.

The AIM analysis confirms the bond formation between O1 and Fe and the peroxide bond cleavage in the reaction path (see Figure 9). As can be seen in Table 1, **C2** presents a BCP for the O1−Fe bond with a low value of $\rho(r)$. At **TSC2-4f** this value has slightly increased and at **4f** a larger value is found. The $E_d(r)$ of this BCP has a positive value at **C2** and a negative value at **TSC2-4f** and evolves to a more stable value for the product. On the other hand, the peroxide bond breaks in this reaction, the $\rho(r)$ changes from 0.248 au at **C2** to 0.168 au at the transition state, while at **4f** no BCP has been found between the two oxygen atoms. Furthermore, the $E_d(r)$ results reveal the loss of stability of this peroxide bond, going from −0.143 au in reactants to −0.056 au at the transition state. $\nabla^2\rho(r)$ presents a more positive value for the transition state than for **C2**, meaning that the BCP is in a region with more charge depletion. This trend, together with the $\rho(r)$ and $E_d(r)$ results, describes the O1−O2 cleavage.

Looking at the contour maps of the electron density Laplacian, it is worth noting that, at **1f**, **C1**, and **C2**, the charge concentration zones around the oxygens O1 and O2 present a protruding region pointing to the BCP. Such regions correspond to the electron density belonging to the monosynaptic basins located between O1 and O2 in the ELF study. The corresponding contour maps of **TSC1-3f**, **TSC2-4f**, **3f**, and **4f** show the disappearance of this protuberance, due to the drop of the electron density in this region.

Topological Description of TS4f-6f and 6f. The ELF analysis of **4f** shows a disynaptic basin between the C3 and C4 cores with a population of 1.61 electrons. This basin disappears

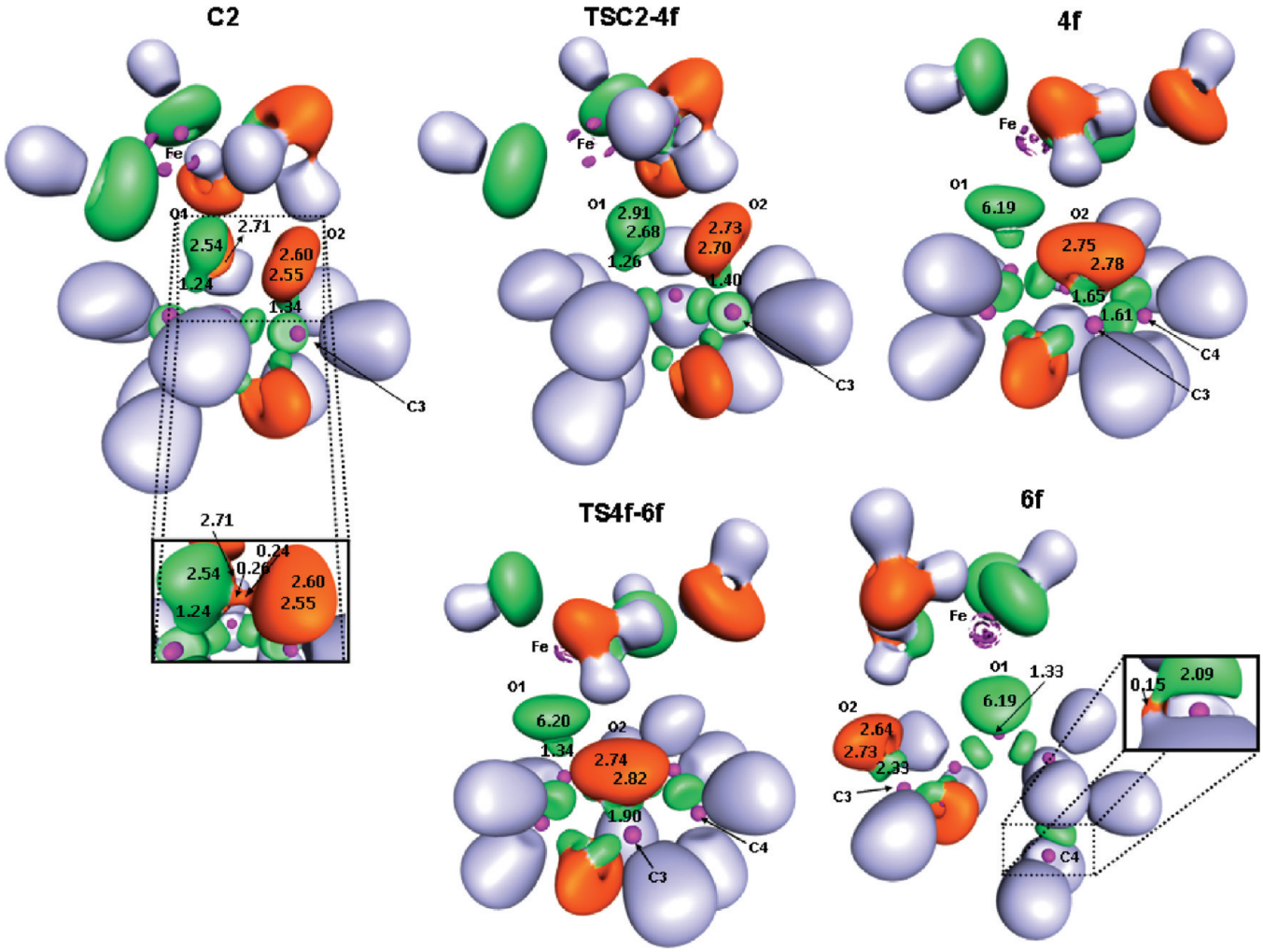

Figure 8. ELF isosurfaces of **C2**, **TSC2-4f**, **4f**, **TS4f-6f**, and **6f**.

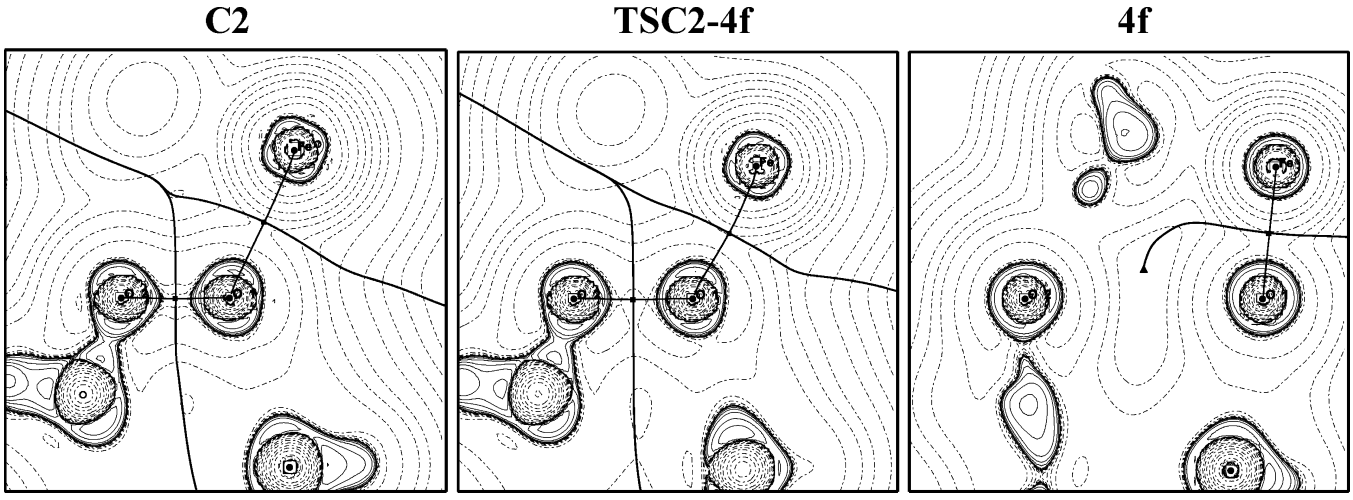

Figure 9. Contour maps of the Laplacian of the electron density for the indicated stationary points.

at **TS4f-6f**, indicating the C3−C4 bond cleavage. In this transition state the population of the disynaptic basin between the O2 and C3 cores increases with respect to **4f**, showing a value of 1.90 electrons. At **6f** the O2−C3 basin has a population of 2.33, and the lone pairs of O2 present charge excess (2.64 and 2.73 electrons). In this structure, the C-radical character is proven with the formation of an unshared basin of 0.15 electrons in C4 and the increase of the population of the disynaptic basin between C4 and C5, which has a value of 2.09 electrons, far larger than a common C−C bond. Again, the ELF analysis describes the electron flows leading in this case from the O2-centered radical **4f** to the C4-centered radical **6f**.

The C3−C4 bond cleavage and C3−O2 double bond formation can be described on the basis of the AIM analysis. **4f** shows a BCP between C3 and C4 with a value of 0.188 au for $\rho(r)$, which decreases to 0.090 au at the **TS4f-6f** (see Table 1). At **6f** no BCP has been found, because the bond between C3 and C4

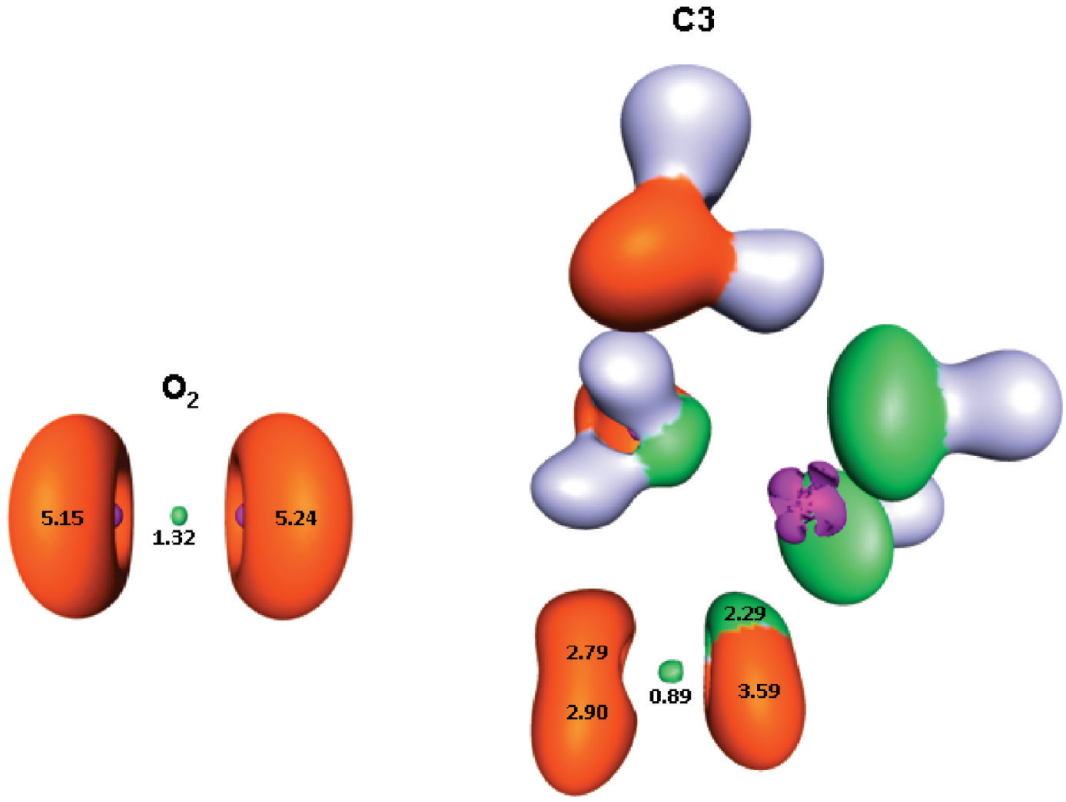

Figure 10. ELF isosurfaces of **C3** and O_2.

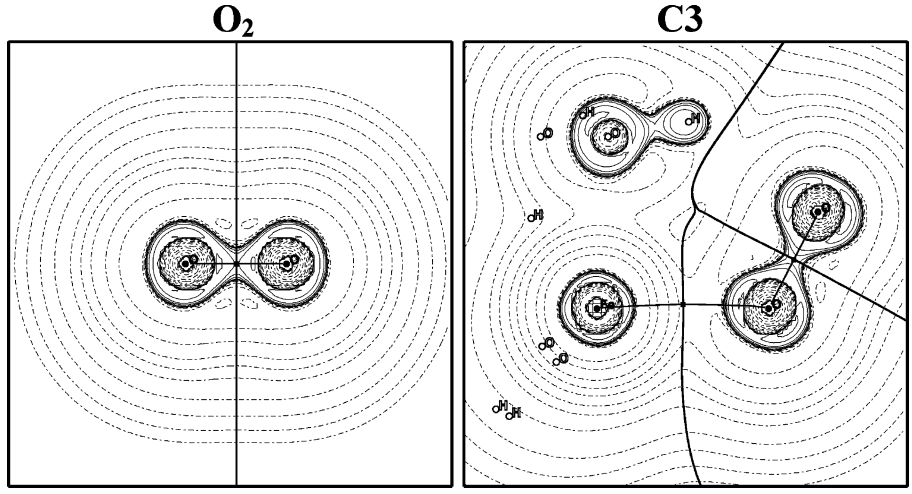

Figure 11. Contour maps of the Laplacian of the electron density for the indicated stationary points.

has been broken. Furthermore, the values of $E_d(r)$ for this BCP change from −0.126 au at **4f** to −0.034 au at the transition state.

In the BCP located between C3 and O2, the $\rho(r)$ is 0.337 au at **4f**, and increases as the reaction takes place, being 0.378 au at **TS4f-6f** and 0.410 au at **6f**. The $E_d(r)$, which has a value of −0.521 au at **4f**, evolves to more stable values of −0.616 and −0.690 au at **TS4f-6f** and **6f**, respectively.

Topological Description of O_2 and C3. The ELF analysis of O_2 shows a disynaptic basin between the oxygen atoms with a population of 1.32 electrons, which reduces to 0.89 electrons at **C3** (see Figure 10). The topology of this bond at **C3** is significantly different of the peroxide bond at **C1** and **C2**, where two monosynaptic basins constituted the protocovalent bond between the peroxide oxygen atoms. On the other hand, a disynaptic basin has been found between the iron atom and the oxygen atom linked to it, showing a population of 2.29 electrons. The monosynaptic unshared basins on the oxygen atoms at O_2 have a population of 5.15 and 5.24 electrons, showing its paramagnetic character. At **C3** the monosynaptic unshared basin of the oxygen linked to Fe has a population of 3.59 electrons, while the unshared basins of the other oxygen atom are overpopulated with 5.69 electrons, due to the radical character of this oxygen atom.

The AIM study of O_2 and **C3** (see Figure 11 and Table 1) points out the presence of a BCP between the oxygen atoms, located in a valence shell charge concentration region as the negative $\nabla^2\rho(r)$ values of −0.765 au for O_2 and −0.317 au for **C3** indicate. The electron density changes from a value of 0.539 au at O_2 to 0.424 au at **C3**, showing the charge delocalization to the oxygen atoms. The highly negative values of the electronic energy density of −0.659 au at O_2 and −0.419 au at **C3**, together

with the aforementioned $\nabla^2\rho(r)$ and $\rho(r)$ values, show the covalent character of the O−O bond. On the other hand, the BCP located between the iron atom and one of the oxygen atoms at **C3** corresponds to an unshared-electron interaction, as the positive value for $\nabla^2\rho(r)$ of 0.314 au, the small value of 0.080 au for $\rho(r)$, and the very small negative value of −0.006 au for $E_d(r)$ indicate.

Moreover, a comparison between the O−O BCP at O_2 and at **1f** reveals that the electron density at O_2 is 0.539 au while at **1f** is only of 0.255 au. The Laplacian at O_2 has a negative value of −0.765 au, and hence the BCP is in a valence shell charge accumulation region, while at **1f** the Laplacian value is positive (0.121 au), and it is in a valence shell charge depletion zone. The electronic energy density shows the O−O bond being more robust at O_2 than at **1f** (−0.659 and −0.152 au, respectively). From these results, it is concluded that the O−O bond at **1f** is much more reactive than at O_2, thus explaining why the ferrous model reacts preferably with the endoperoxide-containing species than with the molecular oxygen.

Conclusions

The present work represents a new contribution to the study of the antimalarial mode of action of artemisinin and focuses on the electronic and topological aspects of the reaction between heme and artemisinin by using very simple molecular models. The key first steps of the artemisinin decomposition induced by Fe(II)-containing species, leading to carbon-centered radicals postulated as the agents responsible of causing the parasite death, have been analyzed with the ELF and AIM methodologies. In this way, following the flows of electron density charge between the ELF basins, a quantitative analysis of the electronic rearrangements along the reaction pathways has been done, and the bond formation/breaking processes have been described.

The reported results explain the affinity between Fe and the peroxide bond. Furthermore, a comparison has been made with the reaction of Fe(II) with molecular oxygen, and from the results obtained it is concluded that the ferrous model reacts preferably with the endoperoxide-containing species. Hence, the disruption by artemisinin of the heme detoxification process would take place by avoiding the initial Fe(II) to Fe(III) oxidation. Artemisinin would compete with molecular oxygen in the very first step of hemozoin formation, killing in this way the malaria parasite. This finding can shed additional light to our current understanding of the antimalarial action of artemisinin and its derivatives.

Some additional specific conclusions can also be derived from this work:

(a) The C4 primary radical **6f** is found to be the most stable structure within the initial steps of the artemisinin decomposition, and hence the O2 radical route is calculated to be thermodynamically, and also kinetically, favored until the C-radicals are formed. This agrees with the fact that the only fully characterized alkylation reaction reported to date in infected mice is the heme alkylation by means of the C4 primary radical.

(b) In spite of the preceding conclusion, the O1 radical route can compete and be also operative, as it was experimentally established.[32,80] The finding that the **C1** complex is more stable than the **C2** gives support to these experimental observations.

(c) The O1−O2 bond in **1f** has been characterized by means of the ELF and AIM analysis as a protocovalent bond, i.e., a bond with a relatively low stability. This is the reason why the endoperoxide bond in artemisinin can be easily broken in the presence of Fe(II) species. On the contrary, the O−O bond in O_2 shows a more populated disynaptic basin, and therefore this bond is described as stronger than the equivalent bond in **1f**. This conclusion is reinforced by the results of the AIM analysis, as the electronic properties for this bond critical point reveal.

(d) It has been found by means of the ELF and AIM study that the cleavage of the artemisinin endoperoxide bond initiates the electronic reorganization leading to the O-centered radicals, in agreement with the experimental observation that the 1,2,4-trioxane ring system is necessary for the antimalarial activity.[4,23]

(e) The ELF analysis accurately describes the electron flows that lead from the reactants to the O-centered radicals, and from these to the C-centered radicals. Furthermore, the AIM study quantitatively accounts for the cleavage/formation of the bonds and provides us a picture at an electronic level of the chemical rearrangements taking place in the processes herein studied.

Further work is required in regard to increasing the molecular model size and accuracy. The way by which the carbon-centered radicals alkylate heme will also be studied. Our group is conducting these studies and the results obtained will hopefully be reported in due form, with the ultimate aim of contributing to a better understanding of the antimalarial activity of artemisinin.

Acknowledgment. Financial support by the Ministerio de Educación y Ciencia (Project CTQ2006-15447-C02-01), Generalitat Valenciana (Projects ACOMP/2009/121 and PROMETEO/2009/053), and Fundació Bancaixa-UJI (P1.1B2008-37 and P1.1B2005-27) is gratefully acknowledged. P.M. acknowledges the Universitat Jaume I for the grant PREDOC/2005/28. A.S.-G. acknowledges the grant associated with the project P1.1B2005-27.

References and Notes

(1) Tonmunphean, S.; Parasuk, V.; Kokpol, S. *Bioorg. Med. Chem.* **2006**, *14*, 2082.
(2) O'Neill, P. M.; Posner, G. H. *J. Med. Chem.* **2004**, *47*, 2945.
(3) Posner, G. H.; O'Neill, P. M. *Acc. Chem. Res.* **2004**, *37*, 397.
(4) Meshnick, S. R.; Taylor, T. E.; Kamchonwongpaisan, S. *Microbiol. Rev.* **1996**, *60*, 301.
(5) Jani, D.; Nagarkati, R.; Beatty, W.; Angel, R.; Slebodnick, C.; Andersen, J.; Kumar, S.; Rathore, D. *PLoS Pathogens* **2008**, *4*, e1000053.
(6) Drew, M. G. B.; Metcalfe, J.; Dascombe, M. J.; Ismail, F. M. D. *J. Med. Chem.* **2006**, *49*, 6065.
(7) Pereira, M. S. C.; Kiralj, R.; Ferreira, M. M. C. *J. Chem. Inf. Model.* **2008**, *48*, 85.
(8) Egan, T. J. *Mol. Biochem. Parasitol.* **2008**, *157*, 127.
(9) Krugliak, M.; Zhang, F.; Ginsburg, H. *Mol. Biochem. Parasitol.* **2002**, *119*, 249.
(10) Goldberg, D. E.; Slater, A. F.; Cerami, A.; Henderson, G. B. *Proc. Natl. Acad. Sci. U.S.A.* **1990**, *87*, 2931.
(11) Kannan, R.; Kumar, K.; Sahal, D.; Kukreti, S.; Chauhan, V. S. *Biochem. J.* **2005**, *385*, 409.
(12) Egan, T. J.; Combrinck, J. M.; Egan, J.; Hearne, G. R.; Marques, H. M.; Ntenteni, S.; Sewell, B. T.; Smith, P. J.; Taylor, D.; van Schalkwyk, D. A.; Walden, J. C. *Biochem. J.* **2002**, *365*, 343.
(13) Rathore, D.; McCutchan, T. F.; Sullivan, M.; Kumar, S. *Expert. Opin. Investig. Drugs* **2005**, *14*, 871.
(14) Cazelles, J.; Robert, A.; Meunier, B. *J. Org. Chem.* **2002**, *67*, 609.
(15) Robert, A.; Cazelles, J.; Meunier, B. *Angew. Chem., Int. Ed.* **2001**, *40*, 1954.
(16) Robert, A.; Meunier, B. *Chem. Soc. Rev.* **1998**, *27*, 273.
(17) Zhang, F.; Gosser, D. K.; Meshnick, S. R. *Biochem. Pharmacol.* **1992**, *43*, 1805.
(18) da Silva Costa, M.; Kiralj, R.; Ferreira, M. M. C. *Quim. Nova* **2007**, *1*, 25.
(19) Mockenhaupt, F. P. *Parasitol. Today* **1995**, *11*, 248.
(20) Haynes, R. K.; Ho, W.-Y.; Chan, H.-W.; Fugmann, B.; Stetter, J.; Croft, S. L.; Vivas, L.; Peters, W.; Robinson, B. L. *Angew. Chem., Int. Ed.* **2004**, *43*, 1381.
(21) Krishna, S.; Woodrow, C.; Staines, H. M.; Haynes, R. K.; Mercereau-Puijalon, O. *Trends Mol. Med.* **2006**, *12*, 200.
(22) White, N. J. *J. Clin. Invest.* **2004**, *113*, 1084.
(23) Gu, J.; Chen, K.; Jiang, H.; Leszczynski, J. *J. Phys. Chem. A* **1999**, *103*, 9364.

(24) Robert, A.; Bonduelle, C.; Laurent, S. A.-L.; Meunier, B. *J. Phys. Org. Chem.* **2006**, *19*, 562.
(25) Robert, A.; Benoit-Vical, F.; Claparols, C.; Meunier, B. *Proc. Natl. Acad. Sci.* **2005**, *102*, 13676.
(26) Robert, A.; Dechy-Cabaret, O.; Cazelles, J.; Meunier, B. *Acc. Chem. Res.* **2002**, *35*, 167.
(27) Jefford, C. W. *Curr. Med. Chem.* **2001**, *8*, 1803.
(28) Posner, G. H.; Park, S. B.; González, L.; Wang, D.; Cumming, J. N.; Klinedinst, D.; Shapiro, T. A.; Bachi, M. D. *J. Am. Chem. Soc.* **1996**, *118*, 3537.
(29) Posner, G. H.; Oh, C. H. *J. Am. Chem. Soc.* **1992**, *114*, 8328.
(30) O'Neill, P. M.; Bishop, L. P.; Searle, N. L.; Maggs, J. L.; Ward, S. A.; Park, B. K.; Mabbs, F. *J. Org. Chem.* **2000**, *65*, 1578.
(31) Butler, A. R.; Gilbert, B. C.; Hulme, P.; Irvine, L. R.; Renton, L.; Whitwood, A. C. *Free Rad. Res.* **1998**, *28*, 471.
(32) Wu, W.-M.; Wu, Y.; Wu, Y.-L.; Yao, Z.-J.; Zhou, C.-M.; Li, Y.; Shan, F. *J. Am. Chem. Soc.* **1998**, *120*, 3316.
(33) Eckstein-Ludwig, U.; Webb, R. J.; van Goethem, I. D. A.; East, J. M.; Lee, A. G.; Kimura, M.; O'Neill, P. M.; Bray, P. G.; Ward, S. A.; Krishna, S. *Nature* **2003**, *424*, 957.
(34) Ridley, R. G. *Nature* **2003**, *424*, 887.
(35) Haynes, R. K.; Monti, D.; Taramelli, D.; Basilico, N.; Parapini, S.; Olliaro, P. *Antimicrob. Agents Chemother.* **2003**, *47*, 1175.
(36) Olliaro, P.; Haynes, R. K.; Meunier, B.; Yongyuth, Y. *Trends Parasitol.* **2001**, *17*, 123.
(37) Bhisutthibhan, J.; Meshnick, S. R. *Antimicrob. Agents Chemother.* **2001**, *45*, 2397.
(38) Pandey, A. V.; Tekwani, B. L.; Singh, R. L.; Chauhan, V. S. *J. Biol. Chem.* **1999**, *274*, 19383.
(39) Asawamahasakda, W.; Ittarat, I.; Pu, Y. M.; Ziffer, H.; Meshnick, S. R. *Antimicrob. Agents Chemother.* **1994**, *38*, 1854.
(40) Bhisutthibhan, J.; Philbert, M. A.; Fujioka, H.; Aikawa, M.; Meshnick, S. R. *Eur. J. Cell. Biol.* **1994**, *78*, 665.
(41) Yang, Y. Z.; Little, B.; Meshnick, S. R. *Biochem. Pharmacol.* **1994**, *48*, 569.
(42) Yang, Y. Z.; Asawamahasakda, W.; Meshnick, S. R. *Biochem. Pharmacol.* **1993**, *46*, 336.
(43) Cumming, J. N.; Ploypradith, P.; Posner, G. H. *Adv. Pharmacol.* **1996**, *37*, 253.
(44) Araújo, J. Q.; Carneiro, J. W. d. M.; de Araujo, M. T.; Leite, F. H. A.; Taranto, A. G. *Bioorg. Med. Chem.* **2008**, *16*, 5021.
(45) Nosoongnoen, W.; Pratuangdejkul, J.; Sathirakul, K.; Jacob, A.; Conti, M.; Loric, S.; Launay, J.-M. *Phys. Chem. Chem. Phys.* **2008**, *10*, 5083.
(46) Galasso, V.; Kovac, B.; Modelli, A. *Chem. Phys.* **2007**, *335*, 141.
(47) Drew, M. G. B.; Metcalfe, J.; Dascombe, M. J.; Ismail, F. M. D. *J. Mol. Struct. (THEOCHEM)* **2007**, *823*, 34.
(48) Wiwanitkit, V. *J. Infect.* **2006**, *53*, 148.
(49) Taranto, A. G.; Carneiro, J. W. d. M.; de Araujo, M. T. *Bioorg. Med. Chem.* **2006**, *14*, 1546.
(50) de Araujo, M. J.; de Carneiro, J. W.; Taranto, A. G. *Int. J. Quantum Chem.* **2006**, *106*, 2804.
(51) Drew, M. G. B.; Metcalfe, J.; Ismail, F. M. D. *J. Mol. Struct. (THEOCHEM)* **2005**, *756*, 87.
(52) Arantes, C.; de Araujo, M. J.; Taranto, A. G.; de Carneiro, J. W. *Int. J. Quantum Chem.* **2005**, *103*, 749.
(53) Tonmunphean, S.; Parasuk, V.; Kokpol, S. *J. Mol. Struct. (THEOCHEM)* **2005**, *724*, 99.
(54) Rafiee, M. A.; Hadipour, N. L.; Naderi-manesh, H. *J. Chem. Inf. Model.* **2005**, *45*, 366.
(55) Drew, M. G. B.; Metcalfe, J.; Ismail, F. M. D. *J. Mol. Struct. (THEOCHEM)* **2004**, *711*, 95.
(56) Pinheiro, J. C.; Kiralj, R.; Ferreira, M. C. *QSAR Comb. Sci.* **2003**, *22*, 830.
(57) Taranto, A. G.; Carneiro, J. W. d. M.; de Oliveira, F. G.; de Araujo, M. T.; Correa, C. R. *J. Mol. Struct. (THEOCHEM)* **2002**, *580*, 207.
(58) Tonmunphean, S.; Parasuk, V.; Kokpol, S. *J. Mol. Model.* **2001**, *7*, 26.
(59) Pinheiro, J. C.; Ferreira, M. M. C.; Romero, O. A. S. *J. Mol. Struct. (THEOCHEM)* **2001**, *572*, 35.
(60) Gu, J. D.; Chen, K. X.; Jiang, H. L.; Leszczynski, J. *J. Mol. Struct. (THEOCHEM)* **1999**, *491*, 57.
(61) Moles, P.; Oliva, M.; Safont, V. S. *Tetrahedron* **2008**, *64*, 9448.
(62) Moles, P.; Oliva, M.; Safont, V. S. *J. Phys. Chem. A* **2006**, *110*, 7144.
(63) Zhang, S.; Gerhard, G. S. *Bioorg. Med. Chem.* **2008**, *16*, 7853.
(64) Becke, A. D.; Edgecombe, K. E. *J. Chem. Phys.* **1990**, *92*, 5397.
(65) (a) Silvi, B.; Savin, A. *Nature* **1994**, *371*, 683. (b) Silvi, B.; Fourré, I.; Alikhani, M. E. *Monatsh. Chem.* **2005**, *136*, 855.
(66) Bader, R. F. W. *Atoms in Molecules: A Quantum Theory*; Oxford University Press, Inc.: New York, 1990.
(67) Bader, R. F. W. *Chem. Rev.* **1991**, *91*, 893.
(68) Frisch, M. J.; Trucks, G. W.; Schlegel, H. B.; Scuseria, G. E.; Robb, M. A.; Cheeseman, J. R.; Montgomery J. A., Jr.; Vreven, T.; Kudin, K. N.; Burant, J. C.; Millam, J. M.; Iyengar, S. S.; Tomasi, J.; Barone, V.; Mennucci, B.; Cossi, M.; Scalmani, G.; Rega, N.; Petersson, G. A.; Nakatsuji, H.; Hada, M.; Ehara, M.; Toyota, K.; Fukuda, R.; Hasegawa, J.; Ishida, M.; Nakajima, T.; Honda, Y.; Kitao, O.; Nakai, H.; Klene, M.; Li, X.; Knox, J. E.; Hratchian, H. P.; Cross, J. B.; Bakken, V.; Adamo, C.; Jaramillo, J.; Gomperts, R.; Stratmann, R. E.; Yazyev, O.; Austin, A. J.; Cammi, R.; Pomelli, C.; Ochterski, J. W.; Ayala, P. Y.; Morokuma, K.; Voth, G. A.; Salvador, P.; Dannenberg, J. J.; Zakrzewski, V. G.; Dapprich, S.; Daniels, A. D.; Strain, M. C.; Farkas, O.; Malick, D. K.; Rabuck, A. D.; Raghavachari, K.; Foresman, J. B.; Ortiz, J. V.; Cui, Q.; Baboul, A. G.; Clifford, S.; Cioslowski, J.; Stefanov, B. B.; Liu, G.; Liashenko, A.; Piskorz, P.; Komaromi, I.; Martin, R. L.; Fox, D. J.; Keith, T.; Al.Laham, M. A.; Peng, C. Y.; Nanayakkara, A.; Challacombe, M.; Gill, P. M. W.; Johnson, B.; Chen, W.; Wong, M. W.; Gonzalez, C.; Pople, J. A. *Gaussian 03; Revision B.04*; Gaussian, Inc.: Wallingford, CT, 2004.
(69) Becke, A. D. *J. Chem. Phys.* **1993**, *98*, 1372.
(70) Lee, C. T.; Yang, W. T.; Parr, R. G. *Phys. Rev. B* **1988**, *37*, 785.
(71) McIver, J. W., Jr. *Acc. Chem. Res.* **1974**, *7*, 72.
(72) Fukui, K. *J. Phys. Chem.* **1970**, *74*, 4161.
(73) Biegler-Konig, F.; Schonbohm, J.; Bayles, D. *J. Comput. Chem.* **2001**, *22*, 545.
(74) (a) Noury, S.; Krokidis, X.; Fuster, F.; Silvi, B. *Comput. Chem.* **1999**, *23*, 597. (b) Matito, E.; Silvi, B.; Duran, M.; Sola, M. *J. Chem. Phys.* **2006**; 024301.
(75) Konrad-Zuse-Zentrum B. and Mercury Computer Systems: Amira 4.1, 1995−2006.
(76) Tang, Y.; Dong, Y.; Wang, X.; Sriraghavan, K.; Wood, J. K.; Vennerstrom, J. L. *J. Org. Chem.* **2005**, *70*, 5103.
(77) Sambrano, J. R.; Gracia, L.; Andrés, J.; Berski, S.; Beltrán, A. *J. Phys. Chem. A* **2004**, *108*, 10850.
(78) Llusar, R.; Beltrán, A.; Andrés, J.; Noury, S.; Silvi, B. *J. Comput. Chem.* **1999**, *20*, 1517.
(79) Berski, S.; Mierzwicki, K.; Bil, A.; Latajka, Z. *Chem. Phys. Lett.* **2008**, *460*, 559.
(80) Posner, G. H.; Cumming, J. N.; Ploypradith, P.; Oh, C. H. *J. Am. Chem. Soc.* **1995**, *117*, 5885.

JP910207Z